The formation mechanism of the hierarchic microstructure in lath martensite phase and the microstructural evolution in steel
ラスマルテンサイト相の階層構造形成機構の解明とその組織発展過程

Yoshinori MURATA, Graduate School of Engineering, Nagoya University
研究代表者　名古屋大学大学院工学研究科　村田純教

1. Introduction

Martensite phase is classified into several kinds based on the morphology and lattice defects, i.e., thin plate, lens, and lath. Thin plate martensite consists of internal twins and lens martensite contains both internal twins and dislocations. Lath martensite contains only dislocations. In the recent heat-resistant steels, which has high creep strength at elevated temperatures, the carbon content is about 0.1 mass%, where lath martensite always appears. The lath martensite has the unique hierarchical microstructure with high dislocation density and the mechanical properties are related to the microstructure evolution.

It is reported that the lath martensite phase forms in steels having relatively high martensite start (Ms) temperatures and that the habit plane is near $\{557\}_\gamma$ different by about 10 degrees from $\{111\}_\gamma$ [1] [2]. Its crystal-orientation relationship is nearly K-S, composed of the relationships $(111)_\gamma // (011)_{\alpha'}$, $[\bar{1}01]_\gamma // [\bar{1}\bar{1}1]_{\alpha'}$, where $(111)_\gamma$ and $(011)_{\alpha'}$ are close-packed planes and $[\bar{1}01]_\gamma$ and $[\bar{1}\bar{1}1]_{\alpha'}$ are close-packed directions in the austenite phase (γ) and the martensite phase (α′), respectively. A total of 24 crystallographic variants satisfy this orientation relationship as shown in Table 1.

The lath martensite phase possesses a hierarchic structure as follows: (i) A prior austenite grain is composed of *packets*; (ii) A packet is composed of an ensemble of grains, called blocks, which have the same $\{111\}_\gamma$ plane as does the habit plane; and (iii) A block is composed of an ensemble of single martensite crystals called laths, which have nearly the same crystal orientation and high dislocation densities [3] [4].

Crystal orientation in the lath martensite phase was recently analyzed over a relatively wide area using the electron back-scattering pattern (EBSP) measured with a scanning electron microscope (SEM). Morito et al. found that crystal orientation in low-carbon steels deviates locally at each point in a block, and that blocks are composed of not just one but rather a combination of two specific crystallographic variants [2] [3] . For example, grains belonging to variant 4 (V4) are observed only in blocks that are composed predominantly of variant 1 (V1); similarly, grains belonging to variant 5 (V5) are observed only in blocks that are composed predominantly of variant 2 (V2) and so on. The boundary between V1 and V4 in the figure, drawn is the block boundary and this is called as *sub-block* boundary and is distinguished from conventional blocks [2] [3].

Table 1 All 24 crystallographic variants that satisfy the K-S orientation relationship

Variant	Plane parallel	Direction parallel	Variant	Plane parallel	Direction parallel
V1	$(111)_\gamma // (011)_{\alpha'}$	$[\bar{1}01]_\gamma // [\bar{1}\bar{1}1]_{\alpha'}$	V13	$(\bar{1}11)_\gamma // (011)_{\alpha'}$	$[0\bar{1}1]_\gamma // [\bar{1}\bar{1}1]_{\alpha'}$
V2		$[\bar{1}01]_\gamma // [\bar{1}1\bar{1}]_{\alpha'}$	V14		$[0\bar{1}1]_\gamma // [\bar{1}1\bar{1}]_{\alpha'}$
V3		$[01\bar{1}]_\gamma // [\bar{1}\bar{1}1]_{\alpha'}$	V15		$[\bar{1}0\bar{1}]_\gamma // [\bar{1}\bar{1}1]_{\alpha'}$
V4		$[01\bar{1}]_\gamma // [\bar{1}1\bar{1}]_{\alpha'}$	V16		$[\bar{1}0\bar{1}]_\gamma // [\bar{1}1\bar{1}]_{\alpha'}$
V5		$[1\bar{1}0]_\gamma // [\bar{1}\bar{1}1]_{\alpha'}$	V17		$[110]_\gamma // [\bar{1}\bar{1}1]_{\alpha'}$
V6		$[1\bar{1}0]_\gamma // [\bar{1}1\bar{1}]_{\alpha'}$	V18		$[110]_\gamma // [\bar{1}1\bar{1}]_{\alpha'}$
V7	$(1\bar{1}1)_\gamma // (011)_{\alpha'}$	$[10\bar{1}]_\gamma // [\bar{1}\bar{1}1]_{\alpha'}$	V19	$(11\bar{1})_\gamma // (011)_{\alpha'}$	$[\bar{1}10]_\gamma // [\bar{1}\bar{1}1]_{\alpha'}$
V8		$[10\bar{1}]_\gamma // [\bar{1}1\bar{1}]_{\alpha'}$	V20		$[\bar{1}10]_\gamma // [\bar{1}1\bar{1}]_{\alpha'}$
V9		$[\bar{1}\bar{1}0]_\gamma // [\bar{1}\bar{1}1]_{\alpha'}$	V21		$[0\bar{1}\bar{1}]_\gamma // [\bar{1}\bar{1}1]_{\alpha'}$
V10		$[\bar{1}\bar{1}0]_\gamma // [\bar{1}1\bar{1}]_{\alpha'}$	V22		$[0\bar{1}\bar{1}]_\gamma // [\bar{1}1\bar{1}]_{\alpha'}$
V11		$[011]_\gamma // [\bar{1}\bar{1}1]_{\alpha'}$	V23		$[101]_\gamma // [\bar{1}\bar{1}1]_{\alpha'}$
V12		$[011]_\gamma // [\bar{1}1\bar{1}]_{\alpha'}$	V24		$[101]_\gamma // [\bar{1}1\bar{1}]_{\alpha'}$

Many theories regarding the deformation geometry of martensitic transformation, such as Bowles–MacKenzie (BM) theory and Wechsler–Lieberman–Read (WLR) theory, have been proposed [5][6]. They are collectively called the *phenomenological theory of martensite crystallography* (PTMC). PTMC is based on the experimental observation that deformation with martensitic transformation is invariant plane deformation, because the martensite phase maintains continuity with the surrounding austenite phase. As a result, the martensite phase has the invariant plane as the habit plane. In PTMC, all deformations induced by martensitic transformation are explained by a combination of lattice deformation (as crystal structure changes), lattice-invariant deformation occurring from shear deformations and rigid-body rotation. Well-known examples applying PTMC to lath martensite include studies by Sandvik and Wayman, and Kelly [7][8]. However, it is unlikely that transformation actually occurs in this sequence. In other words, PTMC describes the result of transformation well but does not explain the mechanism of transformation.

Khachaturyan has presented a model describing deformation with martensitic transformation [9]. His model considers all deformations to be a combination of lattice deformation (as crystal structure changes from fcc to bct) and lattice-invariant deformations with plastic deformations by slip. This model is reasonable in its explanation of the transformation mechanism, but has not yet been verified by detailed, quantitative analyses. Also, as far as we know, there is no report of the plastic deformation that considers several slip systems independently. Furthermore, it remains unclear why the lath martensite phase should contain sub-blocks as reported by Morito et al., although the lath martensitic structure is important for its contribution to the strength of steel. Thus, it is important for both practical and academic reasons to clarify the mechanism by which the structure forms.

Recently, we clarified the formation mechanism of lath martensite by presenting two types of slip deformation (TTSD) model [10] by extending Khachaturyan's slip deformation model. The purpose of this study is to characterize the microstructure of lath martensite phase by means of simulation. In this simulation, the martensitic transformation in Fe-0.1C mass% lath martensitic steel is simulated by the elasto-plastic phase-field model based on the TTSD model. The establishment of this elasto-plastic phase-field model is to prove the validity of the TTSD model on explaining the formation of lath martensite. On the other hand, the microstructure evolution of lath martensite is presented in 3-D space by the phase-field simulation.

2. Calculation method

Based on the TTSD model [10], an elasto-plastic phase-field model is developed by considering both of the Bain deformation and plastic deformation. For the phase-field model, a field variable $\phi_i(\mathbf{r})\left(i=1,2,3\right)$ is introduced to describe the Bain deformation. $i=1,2,3$ is used to distinguish the three cases of coordinate coincidences and $\mathbf{r}$ is the coordinate vector. The eigenstrain caused by the Bain deformation $\varepsilon_{kl}^{B}(i)(i=1,2,3)$ is listed in matrix form as

$$\varepsilon_{kl}^{B}(1)=\begin{pmatrix}\sqrt{2}a_{\alpha'}/a_{\gamma}-1 & 0 & 0\\ 0 & \sqrt{2}a_{\alpha'}/a_{\gamma}-1 & 0\\ 0 & 0 & c_{\alpha'}/a_{\gamma}-1\end{pmatrix}, \tag{1}$$

$$\varepsilon_{kl}^{B}(2)=\begin{pmatrix} c_{\alpha'}/a_{\gamma}-1 & 0 & 0 \\ 0 & \sqrt{2}a_{\alpha'}/a_{\gamma}-1 & 0 \\ 0 & 0 & \sqrt{2}a_{\alpha'}/a_{\gamma}-1 \end{pmatrix}, \tag{2}$$

$$\varepsilon_{kl}^{B}(3)=\begin{pmatrix} \sqrt{2}a_{\alpha'}/a_{\gamma}-1 & 0 & 0 \\ 0 & c_{\alpha'}/a_{\gamma}-1 & 0 \\ 0 & 0 & \sqrt{2}a_{\alpha'}/a_{\gamma}-1 \end{pmatrix}, \tag{3}$$

where a_{γ} is the lattice parameter of the austenite phase, $a_{\alpha'}$ and $c_{\alpha'}$ are the lattice parameters of the martensite phase, respectively. With respect to plastic deformation, the other field variable $p_i^{\alpha}(\mathbf{r})(i=1,2,3)$ is introduced to characterize the values of local plastic strain produced by dislocations from a specific slip system, where α is the number of slip systems. When α is equal to 1 or 2, it corresponds to the slip system $[101](\bar{1}01)_{\alpha'}$ or $[\bar{1}01](101)_{\alpha'}$, respectively. p_i^{α} is defined as [11]

$$p_i^{\alpha}=\frac{|\mathbf{b}_i|}{m_i^{\alpha}\bullet d_{hkl}}(i=1,2,3). \tag{4}$$

Here, $|\mathbf{b}_i|$ is the absolute value of the Burgers vector, m_i^{α} is the number of lattice planes between two adjacent slip planes in each slip system, and d_{hkl} is the distance between $(hkl)_{\alpha'}$ planes.

The eigenstrain tensor ε_{kl}^{P}, caused by plastic deformation can be written as [11]

$$\varepsilon_{kl}^{P}=\sum_{\alpha}\frac{\mathbf{b}_i^{\alpha}\otimes\mathbf{n}_i^{\alpha}+\mathbf{n}_i^{\alpha}\otimes\mathbf{b}_i^{\alpha}}{2|\mathbf{b}_i^{\alpha}|}\cdot p_i^{\alpha}(\mathbf{r})(i=1,2,3), \tag{5}$$

where $\mathbf{b}_i^{\alpha}$ is the Burgers vector, $\mathbf{n}_i^{\alpha}$ is the unit vector of the slip plane normal, and $\otimes$ represents the dyadic product.

The martensitic transformation is a minimization process of the total free energy, which is defined as the sum of the chemical free energy E_{chem}, gradient energy E_{grad}, and elastic strain energy E_{el} [12]:

$$E_{total}=E_{chem}(\{\phi_i(\mathbf{r})\})+E_{grad}(\{p_i^{\alpha}(\mathbf{r})\})+E_{el}\left(\{\phi_i(\mathbf{r})\},\{p_i^{\alpha}(\mathbf{r})\}\right). \tag{6}$$

Eq. (6) indicates that the chemical free energy is involved in Bain deformation, the gradient energy is involved in plastic deformation, and the elastic strain energy is related both with Bain deformation and dislocation slip.

The dynamics of the martensitic transformation is controlled by the Allen-Cahn equation:

$$\frac{\partial M(\mathbf{r},t)}{\partial t} = -L_M \frac{\delta E_{total}}{\delta M(\mathbf{r},t)}, \tag{7}$$

where $M(\mathbf{r},t)$ ($M = \phi_i, p_i^\alpha$) are the field variables and L_M is the kinetic parameter of each field variable.

3. Results and Discussion

Fig. 1 shows the simulation result of time evolution of three types of blocks in a packet on the <111> plane. The blue areas represent the retained austenite phase and the other colored areas (green, yellow, and red) represent three different block as explained in the formation mechanism of lath martensite. The occurrence of each block is determined by the value of the field variable $\phi_i(\mathbf{r})$. In this simulation, it is assumed that the martensite phase appears only when $\phi_i(\mathbf{r}) \geq 0.7$. As shown in Fig. 1 that at $t^* = 2$, all of the three blocks appear around the dislocation loop set in the center of packet. At $t^* = 4$, different blocks grow bigger around the existing martensite phase. In the process of martensite growth, when a second order block meets a first order block, it will stop growing. It results in that the boundary of the first order block is a straight line. In this manner, the martensite phase becomes coarser until the morphology of the full martensite appears. At $t^* = 8$, the packet is almost full of lath martensite phase except that only a few austenite phase can be seen. At $t^* = 20$, the three blocks have occupied the whole packet, indicating the accomplishment of the martensitic transformation.

Fig. 2 shows the simulation results of time evolution of lath variants in a packet on the <111> plane and the six colored areas represent the six variants which are illustrated explicitly in (e). As shown in Fig. 2 (e), each block shown in Fig. 1 is composed of a pair of variants, i.e., V1~V4, V2~V5, and V3~V6, which is the so-called sub-block structure in lath martensite. A block composed of the two martensitic variants defined by the K-S relationship is ideal for the adjustment of plastic deformation by the two types of slip systems. For comparing, the experimental result is shown in (f), which is the EBSP observation of lath martensite [3]. In Fig. 2(f), the parallel blocks structure can be observed and each block is a combination of two variants. By comparing Figs. 2(e) and (f), the qualitative similarity of the sub-block microstructure between the simulation results and experimental observation can be seen. The ratio of the volume fraction of the three block in our simulation is calculated to be 1:1:1 by the mesh method, while the ratio of B1:B2:B3 in (f) is calculated to be 1:2:1. As the lath martensite is an inhomogeneous system, it needs a lot of mapping information for the accurate quantitative analysis, which is unavailable up to present and needs further effort.

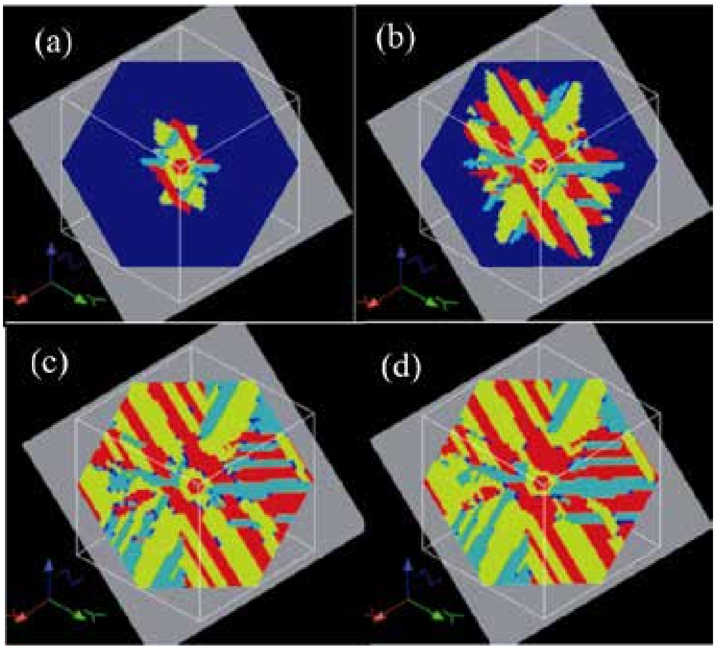

Fig. 1 Time evolution of blocks on <111> plane for (a) t^* = 2, (b) t^* = 4, (c) t^* = 8, and (d) t^* = 20 simulated by elasto-plastic phase-field model. The three colors, i.e., blue, red, and yellow represent three blocks and deep blue represents austenite phase.

Figs. 3 and 4 show the simulation results of the time evolution of plastic strain $p_i^{\alpha}(\mathbf{r})$ along the slip systems of $[101](\bar{1}01)_{\alpha'}$ and $[\bar{1}01](101)_{\alpha'}$ when $i=1$ in a packet, respectively. The blue areas indicate no slip deformation, while the red areas represent the most dramatic slip deformation. Each point in Figs. 3 and 4 represent a local plastic strain for a certain *i*, while all the points scattered in a packet contain the plastic strain coming from the three cases of lattice corresponding, i.e., $i=1$, 2 and 3. The slip systems $[101](\bar{1}01)_{\alpha'}$ and $\left[\bar{1}01\right](101)_{\alpha'}$ correspond to the slip systems when $i=1$. These figures reveal that the plastic deformation originated from the center of the austenite phase and the range of the slip deformation extends with the progression of martensitic transformation. By comparing Figs. 3 and 4, it is found that the plastic deformation along the two slip systems is complementary with each other. Taking area "A" in Fig. 3 and area "B" in Fig. 4 as an example, the plastic strain in "A" is very large, while there is almost no plastic deformation in the same area along the other slip system, as shown in "B". These phenomena can be observed at all places and times during martensitic transformation. So it is concluded that the slip deformation along the two slip systems cooperated with each other to assist the plastic accommodation. The phenomenon that the plastic deformation occurs along the two slip systems alternatively is consistent with the original formation mechanism of lath martensite. It is to be noted that the plastic strain shown in Figs. 3 and 4 only represent the local values in the lattice crystal and all of these values should be integrated within the whole crystal to assess the contribution of dislocation slip on plastic accommodation for martensitic transformation.

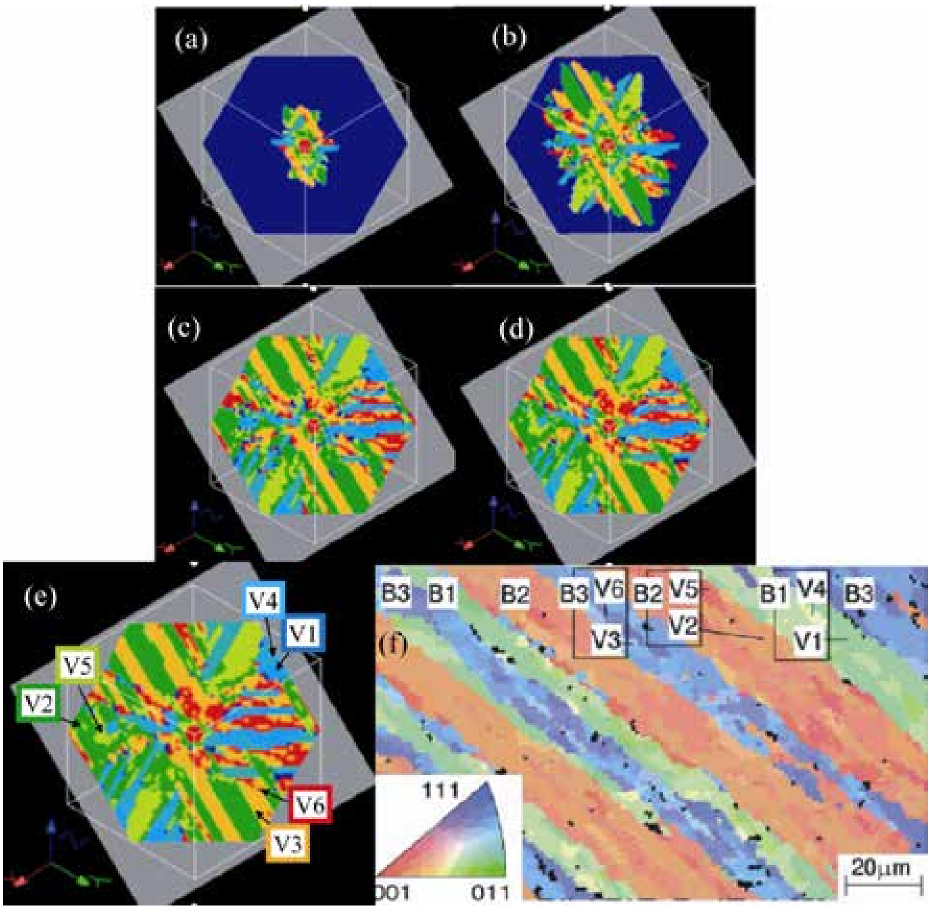

Fig. 2 Time evolution of lath variants on <111> plane for (a) $t^* = 2$, (b) $t^* = 4$, (c) $t^* = 8$, and (d) $t^* = 20$ simulated by elasto-plastic phase-field model. (e) is the specific explanation of variants shown in (d). The six colors represent six different variants in a packet. (f) is the EBSP observation of lath martensite quoted from Ref. [3].

On the other hand, by comparing Fig. 2 and Figs. 3, 4, it is found that the morphology of lath martensite evolution corresponds to the plastic strain evolution. In particular, the slip deformation starts from the beginning of martensitic transformation, as is seen in Figs.3 and 4.

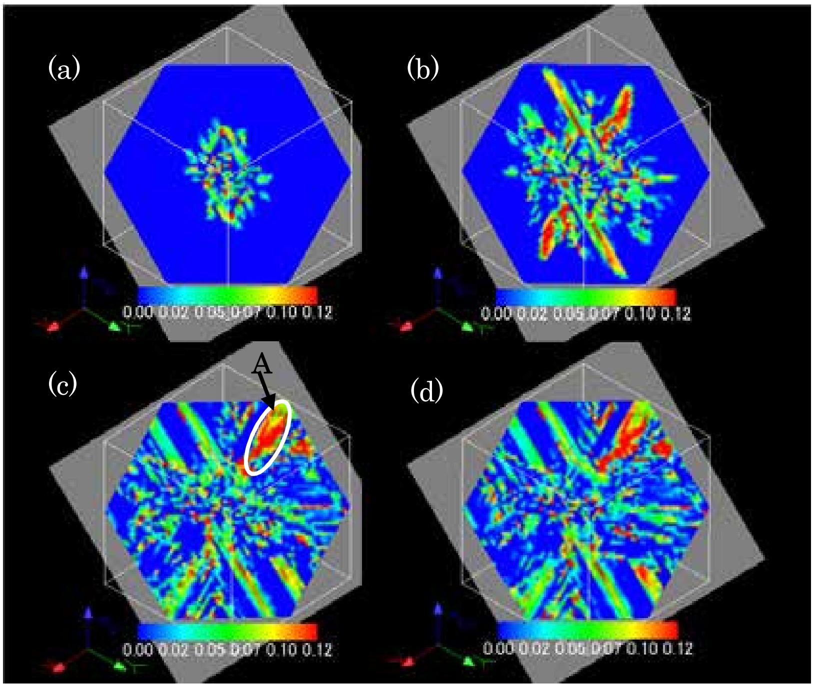

Fig. 3 Time evolution of plastic strain $p_i^{\alpha}(\mathbf{r})(i=1,2,3)$ along $[\bar{1}01](101)_{\alpha'}$ slip system on <111> plane for (a) t^* = 2, (b) t^* = 4, (c) t^* = 8, and (d) t^* = 20 by phase-field simulation.

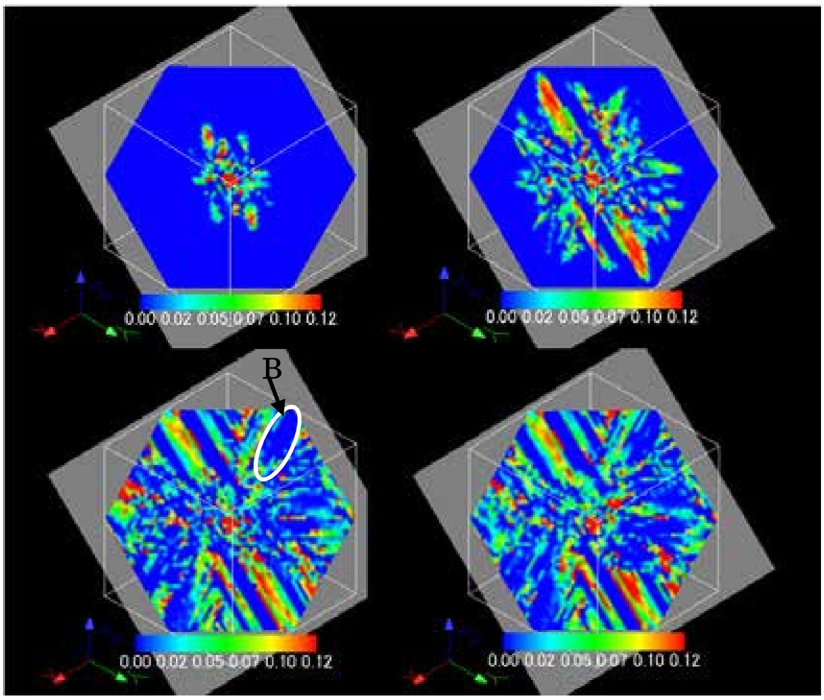

Fig. 4 Time evolution of plastic strain $p_i^{\alpha}(\mathbf{r})(i=1,2,3)$ along $[101](\bar{1}01)_{\alpha'}$ slip system on <111> plane for (a) t^* = 2, (b) t^* = 4, (c) t^* = 8, and (d) t^* = 20 by phase-field simulation.

With the progression of phase transition, the plastic strain increases resulting in the growth and coalescence of the martensitic variants shown in Fig. 2. In other words, the occurrence and evolution of the plastic deformation determine the formation and morphology evolution of the lath martensite phase.

By inserting the local plastic strain along each slip system in Eq. (4), the values of m_1 and m_2 can be evaluated. As mentioned previously, the subscripts 1 and 2 correspond to the $[101](\bar{1}01)_{\alpha'}$ and $[\bar{1}01](101)_{\alpha'}$ slip system $i=1$, respectively. Because of the three cases of lattice corresponding, there should be three pairs of m_1 and m_2. Since each pair is equivalent, only the case in which the $[001]_{\gamma}$-axis coincides with the $[001]_{\alpha'}$-axis, i.e., $i=1$, is discussed as an example. For this case, the variants of V1 and V4 will appear. For the other two cases, the relationship between the values of m along the two independent slip systems should be similar to that of $i=1$. By inserting the local values of the slip deformation p_1^1 and p_1^2 in Eq. (4), the values of m_1 and m_2 are estimated and the relationship between m_1 and m_2 within simulation areas is plotted in Fig. 5(a), where two thousand local values distributed in the simulation areas are collected. It is found that the dense points concentrate in one corner due to the close values as shown in Fig. 5(a). For easy observation, the m_1 and m_2 maxima are limited to within 100 and the enlarged part is shown in Fig. 5(b). For comparison, the analytical result is also shown in Fig. 5(c), which is obtained from eigenvalues satisfying the invariant plane deformation of the deformation matrix [10]. A "corner" type contour is exhibited in Fig. 5(b) and the values of m_1 and m_2 in the corner are approximately 16, which is close to the corner point $m_1 = m_2 = 19$ in Fig. 5(c). Fig. 5(b) also reveals that when m_2 reaches its minimum 10, m_1 increases from 20 to infinity. The converse situation yields a similar result. The contour shown in Fig. 5(b) is consistent with the analytical results shown in Fig. 5(c). This indicates that m_1 and m_2 are mutually dependent, which cannot only be seen from the analytical results, but also from the simulation results. The relationship between m_1 and m_2 corresponds to the relationship between the plastic deformation along the two slip systems. Therefore, it is concluded that the simulation result of the relationship between the two types of slip deformation is consistent with the analytical analysis calculated by the TTSD model. On the other hand, Eq. (4) suggest that if m_1 is larger than m_2, the plastic strain along $[101](\bar{1}01)_{\alpha'}$ is larger than that along $[\bar{1}01](101)_{\alpha'}$. It causes the plastic deformation will be along $[101](\bar{1}01)_{\alpha'}$, resulting in the formation of variant V4. On the contrary, the variant V1 appears. It suggests that the values of m_1 and m_2 determine the appearance of V1 or V4. This simulation result is consistent with the analytical result calculated by Iwashita *et al.* [10].

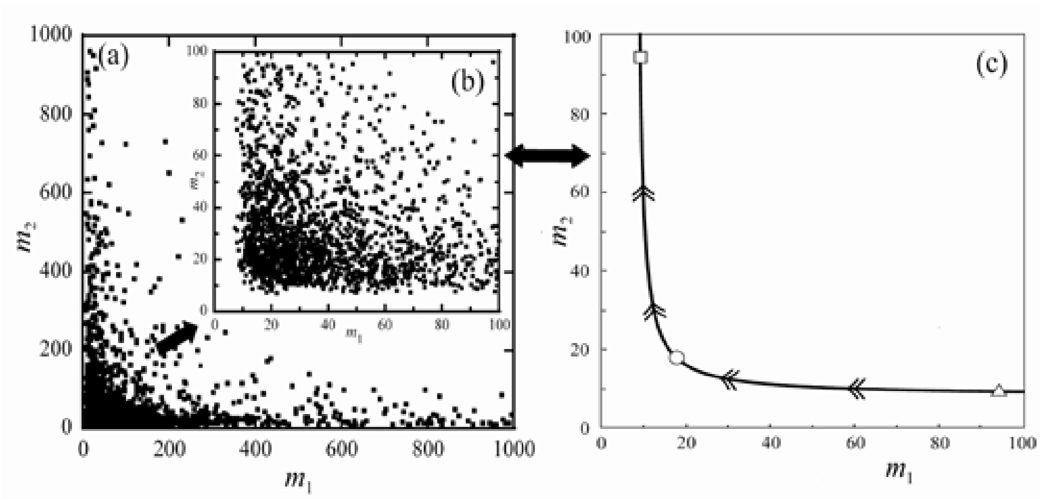

Fig. 5 (a) show the simulation results of the relationship between m_1 and m_2 when i = 1, (b) is the enlarged part of (a) when both of m_1 and m_2 are limited within 100 and (c) is analytical results the relationship between m_1 and m_2 quoted from *Ref*. [10].

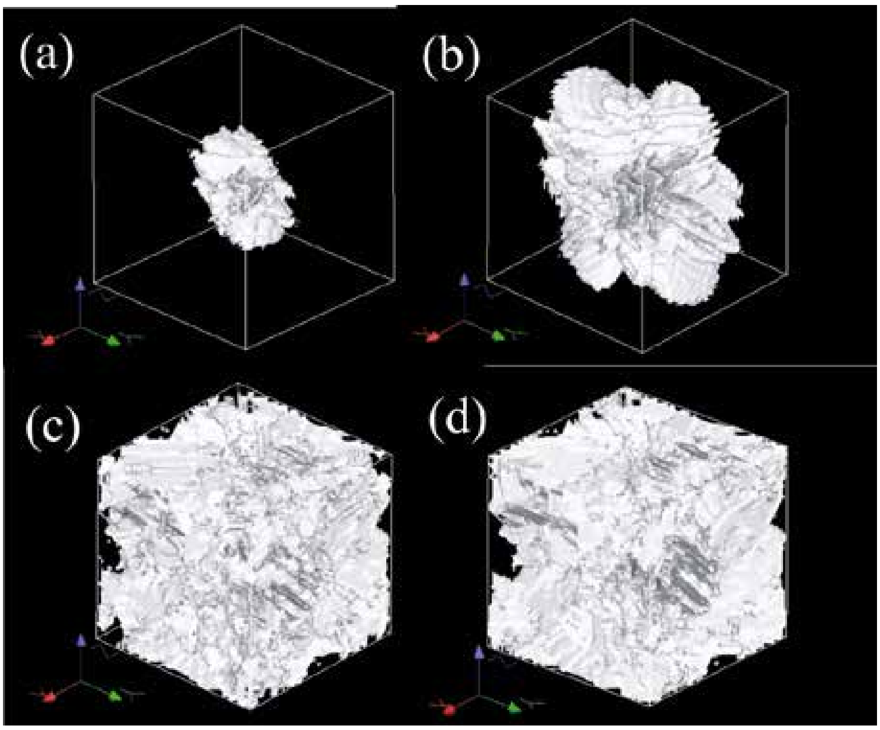

Fig. 6 The growth process of lath martensite at (a) t^* = 2, (b) t^* = 4, (c) t^* = 8, and (d) t^* = 20 in 3-D space simulated by phase-field model.

Fig. 6 shows the growth process of the lath martensite in 3-D space. The cubic skeleton represents the prior austenite lattice. The martensite phase grows bigger around the initial lath martensite nucleus and becomes full martensite at $t^* = 20$, which occupies the whole austenite cubic as shown in Fig. 6(d).

Fig. 7 exhibits the time evolution of lath martensite in 3-D space seen from the outside of austenite cubic. The blue cubic represents the austenite phase lattice. The six coloured areas on the surface of the cubic are the six lath variants. At $t^* = 2$ and 4, the lath martensite only exists inside of the austenite cubic as shown in Figs. 6(a) and (b), resulting in that the lath martensite cannot be seen from the outside. Therefore, the austenite cubic is still blue as shown in Figs. 7(a) and (b). With the progression of the martensitic transition, the lath martensite phase reaches the surface of the austenite cubic and can be seen from the outside of the austenite cubic as shown in Fig. 7(c). When the martensitic transformation is completed, the lath martensite phase spreads all over the surface of austenite cubic as shown in Fig. 7(d).

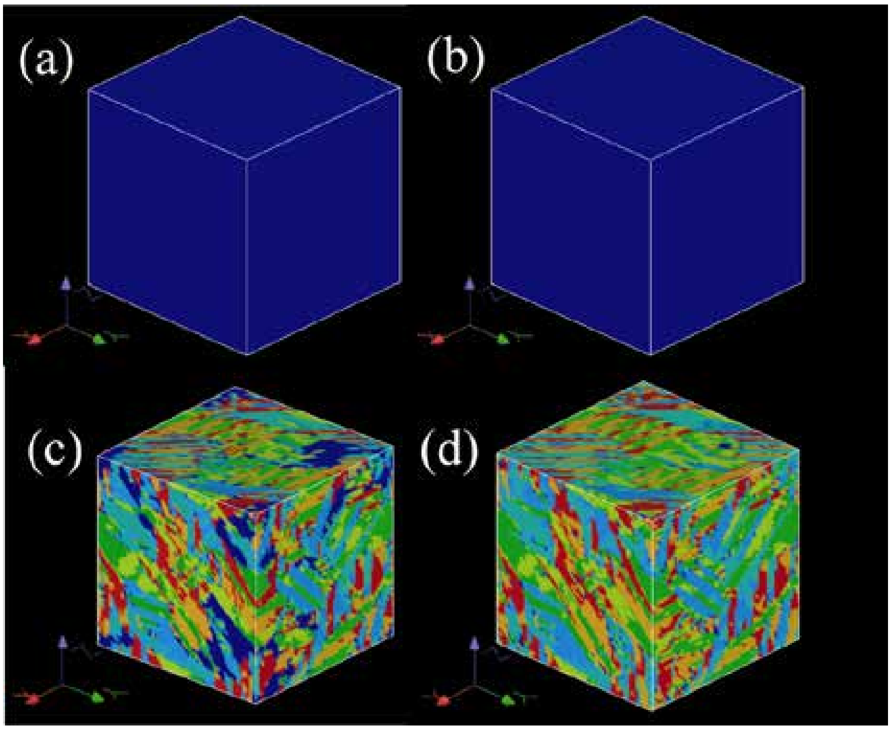

Fig. 7 Time evolution of lath martensite at (a) $t^* = 2$, (b) $t^* = 4$, (c) $t^* = 8$, and (d) $t^* = 20$ in 3-D space observed from the outside of austenite cubic simulated by phase-field model. Each color represents a lath variant.

4. Conclusion

On the basis of the two types of slip deformation (TTSD) model for the formation of lath martensite, an elasto-plastic phase-field model was constructed. Furthermore, the morphology evolution of lath martensite in Fe-0.1C mass% steel was simulated by the elasto-plastic phase-field model in 3-D space. It was observed that the full martensite phase can be obtained by releasing the large elastic strain contained in the Bain deformation, via the two types of independent dislocation slips. Moreover, the morphology of lath martensite such as sub-blocks, as seen in commercial steels, can be well predicted. The relationship of plastic deformation between the two slip systems simulated by phase-field model is consistent with the analytical calculation using by TTSD model. This indicates the validity of the TTSD model for explaining the formation of lath martensite phase.

Acknowledgements

This work was carried out in collaboration with Dr. Yuhki Tsukada (present: Assistant professor of Nagoya Institute of Technology) and was supported by JFE 21st Century Foundation.

References

[1] A.R. Marder and G. Krauss: A.S.M. Transactions quarterly. 62, 4 (1969), 957.
[2] S. Morito, X. Huang, T. Furuhara, T. Maki and N. Hansen,: Acta Materiallia. 54 (2006), 5323.
[3] S. Morito, H. Tanaka, R. Konishi, T. Furuhara and T. Maki,: Acta Materialia. 51 (2003), 1789.
[4] H. Kitahara, R.Ueji, N.Tsuji and Y.Minamino: Acta Materialia. 54 (2006), 1279.
[5] J.S. Bowles, J.K.MacKenzie: Acta Metallurgica. 2 (1954), 129., 138., 224.
[6] M.S. Wechsler, D.S. Lieberman, T.A. Read: Transaction of the American Institute of Mining and Metallurgical Engineers. 197, 11 (1953), 1503.
[7] B.P.J. Sandvik, C.M. Wayman: Metallugical Transactions A. 14A (1983), 835.
[8] P.M. Kelly: Materials Transactions. JIM. 33, 3 (1992), 235.
[9] A.G. Khachaturyan: Theory of Structural Transformations in Solids. New York. Wiley (1983).
[10] K.Iwashita, Y.Murata, Y.Tsukada and T.Koyama, Philos. Mag., 91(2011), pp.4495.
[11] N. Zhou, C. Shen, M. Mills and Y. Wang, Philos. Mag., 90 (2010), pp.405.
[12] Y. Wang and A.G. Khachaturyan, Acta Mater. 45 (1997), pp.759.